Int J Adv Manuf Technol (2008) 37:670–689
DOI 10.1007/s00170-007-1015-y

ORIGINAL ARTICLE

Simulation of dissimilar tailor-welded tubular hydroforming processes using EAS-based solid finite elements

R. A. F. Valente · R. M. Natal Jorge · A. P. Roque · M. P. L. Parente · A. A. Fernandes

Received: 20 June 2006 / Accepted: 13 March 2007 / Published online: 9 May 2007

Abstract Developments in the numerical simulation of the hydroforming process of tubular metallic components, tailor-welded before forming, are presented. Both technologies, *tailor-welded joining operations* and *hydroforming processes*, are well known in industry, although most commonly separately used. Tailor-welded joining operations are usually encountered in plain sheets, subsequently formed by stamping. Tube hydroforming processing, on the other hand, is frequently associated with parts consisting of uniform thickness, material properties, and dimensions. The present analysis focuses on the influence of process parameters, such as the position of the weld-line and initial thickness values, in the innovative process of combining tailor-welded tubes (with distinct thickness values) and hydroforming. Particular attention is posed on the relation of *imposed axial displacement* vs. *imposed hydraulic pressure* into the tube, forming parameters that are not known a-priori in the manufacturing of a new part. Another point of practical interest is the numerical simulation of the weld-line movement, after forming is complete. The finite element method is directly employed in the numerical simulation by means of innovative solid elements suited for incompressibility applications, and included by the authors into the commercial program ABAQUS as *user-elements*. The obtained results can then lead to a better understanding, along with design tools, for the process of hydroforming of tailor-welded tubular parts, accounting for dissimilar thickness of the basic components.

Keywords Tube hydroforming · Tailor-welded tubes · Dissimilar thickness · Weld-line movement · Parameters identification · Numerical simulation

1 Introduction

Tube hydroforming is a forming technique that is increasingly being accepted in the automotive industry, mainly due to the potential advantages such as increased strength and uniformity of final parts, with improved superficial quality and a relative reduction of overall weight. Compared to conventional stamping, tubular hydroformed parts can be obtained with a less number of operations (since the final tubular part can be set in a single stage), therefore reducing the number of secondary operations involved in the manufacturing. The improved surface finishing also introduces less scrap and allows for tighter geometrical tolerances. Nevertheless, the process does have some drawbacks, namely the need for relatively expensive equipment and the higher costs when compared to the rate of production involved. One possible way to lower these costs is the employment of numerical simulation tools for the dies and manufacturing stages design, in order to achieve a better understanding of the whole process. Previous works on the finite element method, for instance, in the simulation

Funding by Ministerio da Ciência, Inovação e Ensino Superior (FCT -Portugal) and FEDER/FSE, under grants POSI SFRH/BD/13013/2003, PTDC/EME-TME/66435/2006 and POCTI/EME/47289/2002, are gratefully acknowledged.

R. A. F. Valente
Department of Mechanical Engineering, University of Aveiro, Aveiro, Portugal

R. M. N. Jorge · A. P. Roque · M. P. L. Parente · A. A. Fernandes
IDMEC-Pólo FEUP, Faculty of Engineering, University of Porto, Porto, Portugal

R. M. N. Jorge (✉)
Department of Mechanical Engineering, University of Porto,
Rua Dr. Roberto Frias, s/n,
4200-465 Porto, Portugal
e-mail: rnatal@fe.up.pt

of hydroforming processes can be found in references [1–8], as well as in some recent works by these authors (see, for example, references [9–11]).

Departing from forming technologies, and turning to the joining of dissimilar blanks, the term "tailor-welded" refers to the class of joining procedures on flat blanks that can be subsequently subjected to forming operations (12–15]). The key idea is to benefit from dissimilar materials and/or thickness values on the initial blank, leading to a sheet forming of composite metallic parts, within single forming operations. As a consequence, this methodology can introduce a higher level of flexibility in manufacturing processes. Another advantage of such a procedure is the relatively low cost of the welding operation over an open sheet blank compared to an equivalent welding procedure performed over an intermediate or final component, after forming stages.

The main purpose of the present work is to provide an analytical framework for the study of a compound manufacturing process, resulting of the application of *hydroforming technologies* over *tailor-welded tubes*, in order to obtain final tubular products consisting of dissimilar materials and/or dissimilar thickness values. The manufacturing of hydroformed tailor-welded tubes can lead to improved, added-value, parts from the point of view of higher strength in zones where structural performance is indeed needed, thus benefiting from a better use of raw materials. Numerical techniques, particularly the finite element method, are used in the present work to simulate the forming of a tailor-welded tubular set, associated with a particular geometry. The heat affected zone (HAZ) is modelled in detail, trying to better reproduce the gradient of material properties, as coming from the welding operation. The key idea here is to provide manufacturing guidelines for this process, particularly by establishing an optimum compromise between the *imposed internal pressure* and *axial feed* (imposed longitudinal displacement) during the hydroforming process. To accomplish this goal, an innovative solid finite element developed by the authors is employed, and integrated as a *user-element* in the commercial software ABAQUS [16]. The finite element formulation is focused in general terms in the following, before introducing the corresponding theoretical background in section 2.

In commercial finite element codes' libraries, it is common to find either shell (or membrane) and continuum (three-dimensional) finite elements. Loosely speaking, the first class is usually employed in the analysis of the deformation of structures with low thickness' values, while the latter element type is conventionally employed in general three-dimensional cases. When relying on a conventional, displacement-based formulation, both shell and three-dimensional elements tend to show numerical pathologies associated with the overestimation of stiffness values, thus leading to the so-called *locking* phenomena.

Transverse shear locking, for instance, is associated with the poor performance of a given finite element formulation in reproducing pure bending situations when low thickness values are involved. *Volumetric locking*, on the other side, is related to the bad quality of results coming from numerical simulation when incompressibility or near-incompressibility models are involved. A comprehensive review of these and other numerical pathologies associated to displacement-based finite element implementations can be found in reference [17].

Related, for instance, to bilinear four-node shell elements, despite the straightforward implementation that is possible to attain, there are a set of limitations that can be pointed out, namely in the analysis and simulation of sheet metal forming. First of all, these kind of elements suffer from a lack of generality, when relying on plane-stress assumptions. That is, a full three-dimensional constitutive law is not directly modelled, causing thickness variations not to be automatically computed from the simulations. Thickness variations can be alternatively obtained, for these cases, by empirical numerical procedures (as in reference [18]) or including into the formulation additional variables (see, for example [19]). Another drawback in conventional shell elements is the impossibility to automatically consider double-sided contact procedures, commonly found in sheet metal forming simulations.

Hexahedral (solid) finite elements are, by essence, able to handle those shortcomings of shell elements, due to the presence of, at-least, eight nodes per element. In this sense, and as real components are by definition three-dimensional parts, these kind of elements might be the natural choice for a simulation. However, in order to obtain reliable results, it is necessary to tackle the locking problems mentioned before, particularly the transverse shear locking (in case low thickness parts are simulated) and volumetric locking (for isochoric plasticity constitutive models). Both pathologies can be dealt with by the use of mixed formulations, as in the case of reduced integration procedures, mixed interpolation of tensorial components, and the enrichment of the polynomials associated with the original (base) displacement field. Details about these (now classical) procedures can be found in a large number of papers in the literature, and comprehensive reviews can be found, for instance, in [20, 21].

In this paper a fully integrated solid element with eight nodes is introduced based on a formulation designed to particularly treat the volumetric and transverse shear locking arising in problems involving isochoric plasticity models. The formulation is based on the use of an *improved enhanced strain* field, when compared to the conventional approach based on the *displacement* field. This methodology is related to what is called the enhanced assumed strain method [22], where a larger subspace basis, thus encom-

passing more incompressible modes of deformation, is sought. The developed solid element is used, in the present work, in the simulation of the hydroforming of tubular parts, as obtained by the tailor-welded union of similar and dissimilar tubes. The geometry of this particular problem is not well suited for a finite element analysis with shell (membrane) elements.

The last statement, moreover, is also justified by the main goals of the present work, which are: (i) the most realistic (as possible) description of the weld zone, including grading of the mechanical properties (only attained by a 3D model of the HAZ); (ii) the characterization of the thickness variations in the formed tubes, as a function of the weld line position and different values of thickness involved; (iii) the prediction of the weld line movement after the hydroforming process.

Taking into account these considerations, and as a summary, the present numerical simulation has the goal to be a design tool in the full characterization of the formed part, along with an aid in the a-priori definition of the incremental process parameters to be used, particularly the external loading and prescribed displacements needed in obtaining a given tailor-welded hydroformed tubular component.

2 Formulation of the EAS solid finite element used

Consider a representative eight node, hexahedral finite element as represented in Fig. 1. Relative to a global orthogonal frame $(\mathbf{e}_1, \mathbf{e}_2, \mathbf{e}_3)$, each point within the element can be defined by a position vector $({}^n\mathbf{x})$, for a given configuration (n), in the form

$$ {}^n\mathbf{x}\left(\xi^1,\xi^2,\xi^3\right) = \frac{1}{2}\left[\left(1+\xi^3\right){}^n\mathbf{x}_t\left(\xi^1,\xi^2\right) + \left(1-\xi^3\right){}^n\mathbf{x}_b\left(\xi^1,\xi^2\right)\right] \tag{1} $$

as a function of the bottom (b) and top (t) projections of the position vector onto the bottom and top surfaces, respectively. It is worth noting that a position vector, for any point within an element, is uniquely defined by the natural set of coordinates $\left(\xi^1,\xi^2,\xi^3\right)$ of the analysed point, as defined over an undeformed unit volume element, that is, an isoparametric mapping in the form

$$ \xi^1,\xi^2,\xi^3 \in [-1,+1]\times[-1,+1]\times[-1,+1] \tag{2} $$

Coherent with the common approach of finite element methodology, a fixed number of interpolation (representative) points within an element are chosen, and a numerical integration procedure is then carried out.

The position vector can also be defined, in a more general way, as a function of the position vectors of each node (i) in the element $\left({}^n\mathbf{x}\left(\xi_i^1,\xi_i^2,\xi_i^3\right)\right)$, as

$$ {}^n\mathbf{x}\left(\xi^1,\xi^2,\xi^3\right) = N_i\left(\xi^1,\xi^2,\xi^3\right){}^n\mathbf{x}\left(\xi_i^1,\xi_i^2,\xi_i^3\right) \tag{3} $$

In the present case, each node corresponds to a vertex point of the hexahedral element, and the summation over

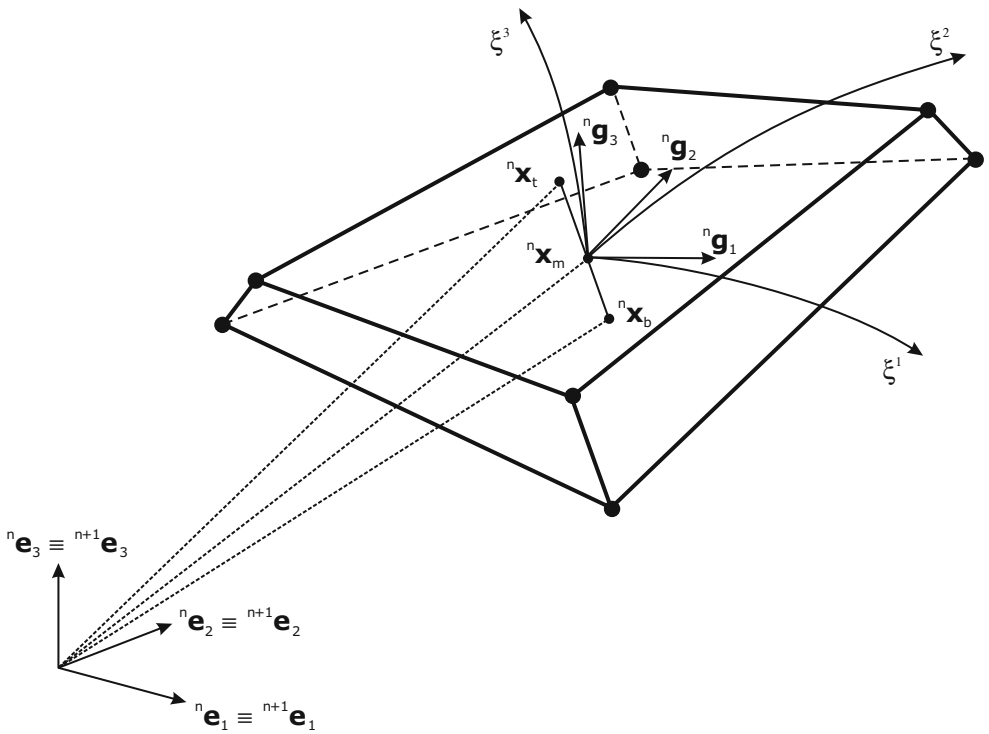

Fig. 1 Representative hexahedral finite element with eight nodes

the number of nodes of the element (i= 1,...,*nnode*) is implicitly defined in Equation (3). Reference source not found.). Additionally in this equation, for the 8-node hexahedral element, shape functions [21] are defined as

$$N_i\left(\xi^1,\xi^2,\xi^3\right)=\frac{1}{8}\left(1+\xi_i^1\xi^1\right)\left(1+\xi_i^2\xi^2\right)\left(1+\xi_i^3\xi^3\right) \tag{4}$$

The parameters involved in Eq. (4) are represented in Table 1.

Deformation process between two configurations (n) and (n+1) can be formulated in terms of displacement variables, coming from successive position vectors (${}^{n}\mathbf{x}$) and (${}^{n+1}\mathbf{x}$), in the form

$${}^{n+1}_{n}\mathbf{u}\left(\xi^1,\xi^2,\xi^3\right)={}^{n+1}\mathbf{x}\left(\xi^1,\xi^2,\xi^3\right)-{}^{n}\mathbf{x}\left(\xi^1,\xi^2,\xi^3\right) \tag{5}$$

representing the displacement field for a specific point $\left(\xi^1,\xi^2,\xi^3\right)$ within the continuum. More insight into the incremental deformation between two configurations can be obtained with the relative deformation gradient

$${}^{n+1}_{n}\mathbf{F}\left(\xi^1,\xi^2,\xi^3\right)=\frac{\partial^{n+1}\mathbf{x}}{\partial^{n}\mathbf{x}} \tag{6}$$

The deformation gradient physically represents the overall deformation of a given body, and can be decomposed in two separated tensors, one $\left({}^{n+1}_{n}\mathbf{R}\right)$ describing the rigid body part of the deformation, inducing rotation but not deformation energy, and a second one $\left({}^{n+1}_{n}\mathbf{U}\right)$ related to the stretch component of the whole deformation

$${}^{n+1}_{n}\mathbf{F}={}^{n+1}_{n}\mathbf{R}\,{}^{n+1}_{n}\mathbf{U} \tag{7}$$

In forming applications, it is usually assumed that the stretch component of deformation in Eq. (7) is relatively small between successive configurations (incremental approach), and an additive treatment of finite strains thus becomes possible. In this case, it is convenient to introduce a *material* measurement of strain, in the form of the Green-Lagrange strain tensor, and calculated based on the displacement field as

$${}^{n+1}_{n}\mathbf{E}=\frac{1}{2}\left({}^{n+1}_{n}\mathbf{F}^{\mathrm{T}}\,{}^{n+1}_{n}\mathbf{F}-\mathbf{I}_2\right) \tag{8}$$

Table 1 Isoparametric indices for Eq. (4)

I	ξ_i^1	ξ_i^2	ξ_i^3
1	−1	−1	−1
2	+1	−1	−1
3	+1	+1	−1
4	−1	+1	−1
5	−1	−1	+1
6	+1	−1	+1
7	+1	+1	+1
8	−1	+1	+1

where ($\mathbf{I}_2$) represents the identity tensor. The Green-Lagrange strain tensor itself consists of a linear part (small deformation field) and a non-linear part (accounting for nonlinear geometric effects), as can be seen in classical texts, such as in [20].

Finite elements entirely based on the displacement field and the Green-Lagrange strain field, are prone to be affected by both *transverse shear* and *volumetric locking* effects, when complete numerical integration rules are used. For the eight-node hexahedral element, this corresponds to numerically evaluate the stiffness matrix coming from the strain field [Eq. (8)] by means of eight interpolation points per element [21]. It is always possible to overcome the locking pathologies using a reduced integration scheme, employing a lower number of interpolation points than theoretically defined. For example, with a single integration point per element it is possible to overcome, to some extent, the locking problem in trilinear solid finite element, although this procedure must be carried out judiciously, to the expenses of introducing spurious (non-physical) deformation modes into the formulation [19]. Therefore, when it is intended to use fully integration procedures, other alternatives must be chosen for locking treatment.

For the present work, the authors employ a fully integrated solid element consisting of eight nodes, and, in order to successfully avoid locking effects, the enhanced assumed strain methodology will be used, as firstly introduced in references [22–24].

In the EAS approach, the strain field directly obtained from the displacements - Eq. (8). - is improved with the inclusion of extra terms, based on a set of element-wise variables. The main procedure is fully detailed in [25] and [26], but for the sake of completeness will be summarized in the following.

The key idea is to improve, as said before, the conventional Green-Lagrange strain field with an enhanced counterpart, within an additive framework, in the form

$$\begin{aligned}{}^{n+1}_{n}\mathbf{E}&=\underbrace{{}^{n+1}_{n}\mathbf{E}^{u}}_{Equation\ (8)}+\underbrace{{}^{n+1}_{n}\mathbf{E}^{\gamma}}_{EAS\ part}\\&={}^{n+1}_{n}\mathbf{E}^{u}+\mathbf{M}^{\gamma}\left(\xi^1,\xi^2,\xi^3\right)\left\{\begin{array}{c}\gamma_1\\ \cdots\\ \gamma_j\end{array}\right\}\end{aligned} \tag{9}$$

where (*EAS*) stands for the enhanced field, introduced into the formulation. In Equation (9), $\left(\mathbf{M}^{\gamma}\left(\xi^1,\xi^2,\xi^3\right)\right)$ represents a strain-displacement matrix relating the Green-Lagrange strain tensor and the enhancing variables set (γ) for the element. The resulting (total) enhanced strain field has the same formal structure of the original one coming from the displacements field (thus turning the implementation straightforward), but designed to successfully avoid the onset of transverse shear and volumetric locking effects.

Focusing now on the particular structure of the strain-displacement matrix $\left(\mathbf{M}^{\gamma}\left(\xi^1,\xi^2,\xi^3\right)\right)$, it was shown in [25] that a possible initial guess for its structure relies in the inclusion of 12 enhancing parameters (j=12 in Eq. (9)). As a result, such a fully integrated element, accounting for an enhanced (final) strain field including this set of variables, shows a robustness to locking effects theoretically equivalent to the one obtained with the use of a reduced integration procedure, but without the drawback of including spurious energetic modes into the formulation.

The particular form of the strain-displacement matrix $\left(\mathbf{M}^{\gamma}\left(\xi^1,\xi^2,\xi^3\right)\right)$, consistent with the use of 12 enhancing variables per finite element, is as follows [25]

$$\mathbf{M}^{\gamma}\left(\xi^1\ \xi^2\ \xi^3\right) = \begin{bmatrix} \frac{\partial N_\alpha}{\partial \xi^1} & & & & & & & & \\ & \frac{\partial N_\alpha}{\partial \xi^2} & & & & & & zeros & \\ & & \frac{\partial N_\alpha}{\partial \xi^3} & & & & & & \\ & & & \frac{\partial N_\alpha}{\partial \xi^1} & \frac{\partial N_\alpha}{\partial \xi^2} & & & & \\ & zeros & & & & \frac{\partial N_\alpha}{\partial \xi^1} & \frac{\partial N_\alpha}{\partial \xi^3} & & \\ & & & & & & & \frac{\partial N_\alpha}{\partial \xi^2} & \frac{\partial N_\alpha}{\partial \xi^3} \end{bmatrix}_{6\times 9} + \begin{bmatrix} \frac{\partial^2 N_\alpha}{\partial \xi^1 \partial \xi^2} & \frac{\partial^2 N_\alpha}{\partial \xi^1 \partial \xi^3} & \frac{\partial^2 N_\alpha}{\partial \xi^2 \partial \xi^3} \\ \frac{\partial^2 N_\alpha}{\partial \xi^1 \partial \xi^2} & \frac{\partial^2 N_\alpha}{\partial \xi^1 \partial \xi^3} & \frac{\partial^2 N_\alpha}{\partial \xi^2 \partial \xi^3} \\ \frac{\partial^2 N_\alpha}{\partial \xi^1 \partial \xi^2} & \frac{\partial^2 N_\alpha}{\partial \xi^1 \partial \xi^3} & \frac{\partial^2 N_\alpha}{\partial \xi^2 \partial \xi^3} \\ & zeros & \end{bmatrix}_{6\times 3} \tag{10}$$

where a new shape function was introduced, in the form

$$N_\alpha = \frac{1}{2}\left(1-\xi^1\xi^1\right)\left(1-\xi^2\xi^2\right)\left(1-\xi^3\xi^3\right) \tag{11}$$

The first sub-matrix in Eq. (10) is obtained from the inclusion of nine enhancing variables, each one related to a term of the *displacement gradient operator*. The sole use of this sub-matrix in the final form of the enhanced strain field is theoretically possible, as shown in [25], although the formulation herein obtained is still susceptible to being affected by locking.

In order to avoid this, and to additionally obtain the same predictability level coming from solid finite elements with reduced formulations, the second sub-matrix is added to the first one, affecting only the direct components of the strain field. More details about this formulation, which gave rise to the so-called *HCi12* solid element, can be found in references [25] and [26]. More details about the mathematical aspects of the EAS formulation, along with the formulation and implementation steps for nonlinear material and geometrical ranges, as developed by authors, can be found in recent works for general thin-shell structures (with emphasis on sheet metal forming applications), as in [27] and [28].

At this point, it is worth mention an important aspect about the present formulation. As described in [25], the use of the specific 12 enhancing variables, as in the equations before, is still grounded in the development of a general-purpose *solid-type* finite element. This fact is compatible with the specific application to be seen in the present paper, particularly focusing on a try to realistically model the HAZ geometry, with grading thickness (and, consequently, mechanical properties), of dissimilar tailor-welded tubular blanks.

Nevertheless, as the thickness of the element becomes increasingly small, the idea itself of providing a three-dimensional formulation may lack some sense, since in this case a shell element (with a well-defined thickness direction) might be used, maybe with relative gains in computation time. Therefore, the present element may not be appropriate for the analysis of extremely thin structures, and must be used carefully in these cases. In these situations, and in order to benefit from both the advantages of a three-dimensional general formulation, but still including thin shell capabilities on it, it is possible to employ an alternative approach like a "solid-shell" formulation, still based on the EAS methodology (see, for instance, [26, 29, 30] and the references herein).

About the implementation of the enhanced solid element into ABAQUS commercial package, a few key points might be highlighted. The user element subroutine is responsible for the definition of the stiffness matrix and internal force vectors at the element level, for each integration point inside the element. In this sense, the constitutive update for material nonlinearities is also performed at the element level, inside the FORTRAN user subroutine. The input parameters to be passed to and from the subroutine are defined by ABAQUS; and in each call of the user element updated nodal coordinates are introduced and historical variables at the integration point's level (stress and strain components, etc) are kept in memory for subsequent cycles. In order to gain computational effectiveness, the strain energy coming from the enhancing parameters, described in the last section, is iteratively calculated up to a predefined tolerance [24], and the enhancing variables are kept at the user-subroutine level, not being stored at the global level. By doing so, the final structure of the assembled stiffness matrix and internal force vector is kept the same as for a conventional solid, eight-node, displacement-based finite element.

3 Problem definition

3.1 Tubular hydroforming example

This section presents an application example consisting of the simulation of the hydroforming process using the enhanced assumed strain (EAS) formulation of the previous

section. The main advantage of using solid elements is the more realistic characterization of the heat affected zone (HAZ) that can be obtained, both in terms of its geometry and mechanical properties, when compared to conventional shell elements, based on plane-stress assumptions and lacking a physical modelling of the thickness dimension.

The study will focus on the analysis of the *deformed shapes*, *final thicknesses*' *values* and *load paths* after hydroforming. The independent variables of the analysis are the *different positions of the weld line* and *distinct initial thickness* for the tailor-welded tube. The weld line movement during forming will be numerically simulated, and the relations between different configurations will be verified ([9–11, 31]).

3.2 Material characterisation for numerical analysis

The geometry to be analysed in the present work was initially introduced in [1], although in the present case a distinguishing feature is considered: the presence of a *weld line* perpendicular to the longitudinal direction of the tube, as can be seen in Fig. 2 [31]. The numerical simulations in this paper were carried out using ABAQUS/Standard software [16], with static implicit non-linear geometric and material features. As mentioned in the previous section, the previously described EAS-based solid element was implemented in ABAQUS as a user element, and the numerical simulation in the following were then run with this software, in order to benefit from its contact algorithms.

Back to the details on the forming process, it mainly consists of inserting the original tubular part inside the tooling set and filling the tube cavity with an incompressible fluid. After this initial stage, internal pressure is further imposed upon the fluid, along with axial displacement in the upper end of the part, which is coincident with the upper surface of the fluid. Therefore, the forming process is driven by the internal pressure (responsible for making the tube material to conform against the die walls) along with the imposed axial displacement, necessary to provide a level of structural instability (wrinkling) on the tube, and thus allowing for a complete pressure forming without rupture. A proper choice and calibration of internal pressure and axial imposed displacement is then needed (most of the time not known for a new product) in order to achieve a flawless final component.

Regarding the configurations of the welded tubes to be hydroformed, three different possibilities exist concerning the shape of the weld line for a butt weld (see Fig. 2), respecting the thickness relations involved in the tailor-welded tube. The choice for *identical average diameters* (as can be seen in Fig. 2b), although easily modelled from the numerical point of view, turns out to be of difficult reproduction in reality. Regarding the two remaining

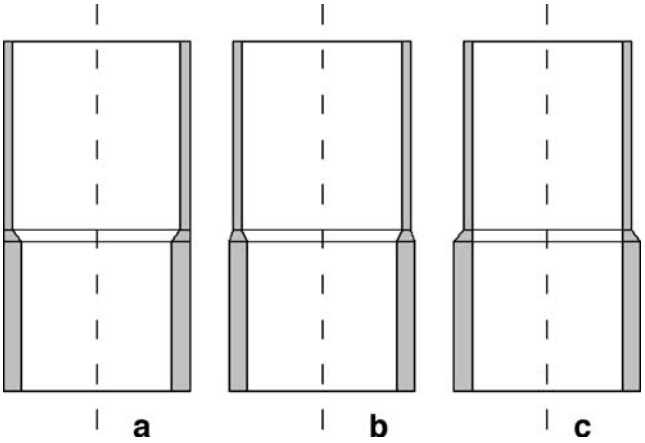

Fig. 2 Possible configurations for butt-welded zones: **a** Common outer diameters; **b** Common average diameters; **c** Common inner diameters

configurations in Fig. 2, they consist of either using *common outer diameters* (as in Fig. 2a) or *common inner diameters* (as in Fig. 2c). For the latter case in Fig. 2c (and also for the identical average diameter in Fig. 2b), there is a lack of contact between the die and the outer zone of the tubular part, along the weld line, which is not desirable. Furthermore, these configurations provide a poor surface finishing, which might impair the applicability of the final part for some applications. For these reasons, the configuration with constant outer diameter, as represented in Fig. 2a, will be the one analysed in the present simulation process.

For the present study, the two tubes to be welded prior to forming have the same material properties, being both tubes of regular steel alloy with elastic mechanical properties as shown in Table 2 [1]. The complete elasto-plastic curve for the tubes' material, relating the equivalent plastic strain and stress and reproducing strain hardening effects, is shown in Fig. 5 (lower curve). Equivalent stress and strain pairs, taken from the previous curve are then introduced in tabular form into ABAQUS software.

The modelling of the weld line mechanical properties, on the other hand, is based on experimental values obtained by micro-hardness essays on heat affected zones (HAZ), as described in [32]. Following this reference, the constitutive properties for the weld zone can then be indirectly obtained in comparison to those of the base material far from the HAZ. In doing so, from [32] a linear relation between the

Table 2 Mechanical properties for the base material of the tubes (steel alloy)

Elastic mechanical properties	
Young modulus	210 GPa
Uniaxial yield stress	136 MPa
Poisson's ratio	0.3

yield stress (σ_y) of the weld region and its counterpart for the base (tube) material is derived in the form:

$$\sigma_y^{weld} = \sigma_y^{tube} \frac{\mathrm{HV}^{weld}}{\mathrm{HV}^{tube}} \tag{12}$$

where *HV* represents micro-hardness values measured in welded (*weld*) and base material regions (*tube*). The obtained values for hardness, for the same materials as seen here, are represented in Fig. 3 [32]. The observed hardening variation in the neighbourhood of the weld center, as represented in Fig. 3, is then used to obtain the values of the yield strength in the entire weld zone by defining different regions along the longitudinal direction of the tube (Fig. 4), with the corresponding differences in the yield stress following from Eq. (12). The resultant stress–strain relations for each representative region of the weld zone are then indicated in Fig. 5. These grading effects in mechanical properties were considered in the present simulation in order to better reproduce the influence of the HAZ in the overall forming operation. Once again, it is worth mentioning that the correct geometric and material modelling for simulation is only attainable with the use of solid elements, in opposition of shell elements based on plane stress assumptions (and no physical thickness dimensions' representation), as commonly found in commercial finite element packages.

Another point worth mentioning in Fig. 5 is related to the stress–strain relation for the plastic domain, including hardening effects, for each of the distinct zones in the welding region. In the present work, a simplified model of hardening was assumed, relying on the behaviour of the base metal. In this sense, the deformation-based hardening along the welding zone is assumed to show the same evolution with the plastic strain field, as the one corresponding to the base material.

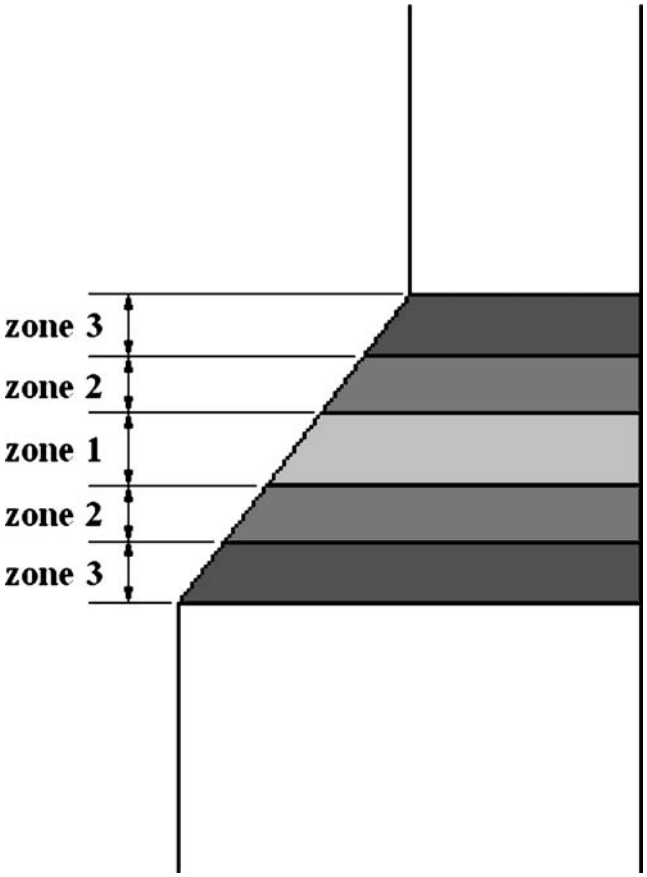

Fig. 4 Grading of mechanical properties along the weld region direction

3.3 Study cases

After choosing the welding configuration model to be simulated, along with the corresponding constitutive prop-

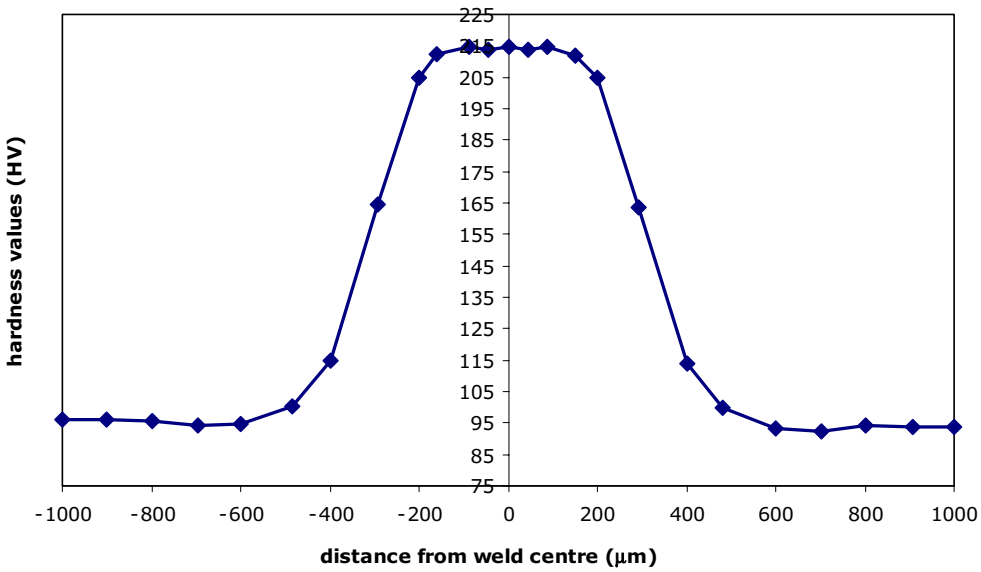

Fig. 3 Hardness distribution in the weld region (obtained from [32])

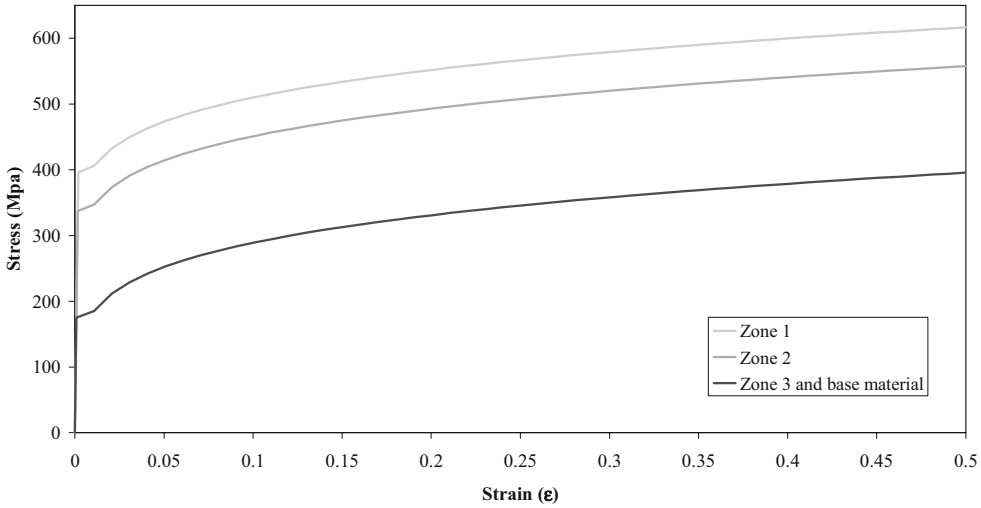

Fig. 5 Equivalent stress–strain relations used for the base and heat affected zone materials

erties gradient along the heat affected zone, it is necessary to specify the set of forming parameters to be studied.

Regarding the location of the weld-line in the initial (undeformed) tailor-welded tube, three different positions along the longitudinal direction were considered in the simulation, as represented in Fig. 6. The corresponding longitudinal coordinates for the weld lines measured from the bottom of the initial tube (along Y direction in the figure) are indicated in Table 3.

Apart from the weld line location, distinct ratios between thickness' values were also considered in the simulation, corresponding to tailor-welded models with dissimilar thickness values of: (a) 1.2–1.8 (mm), and (b) 1.2–2.4 (mm). In these cases, the largest thickness is placed under the weld line, while the smallest thickness is located above the weld line (as in Figs. 2 and 4).

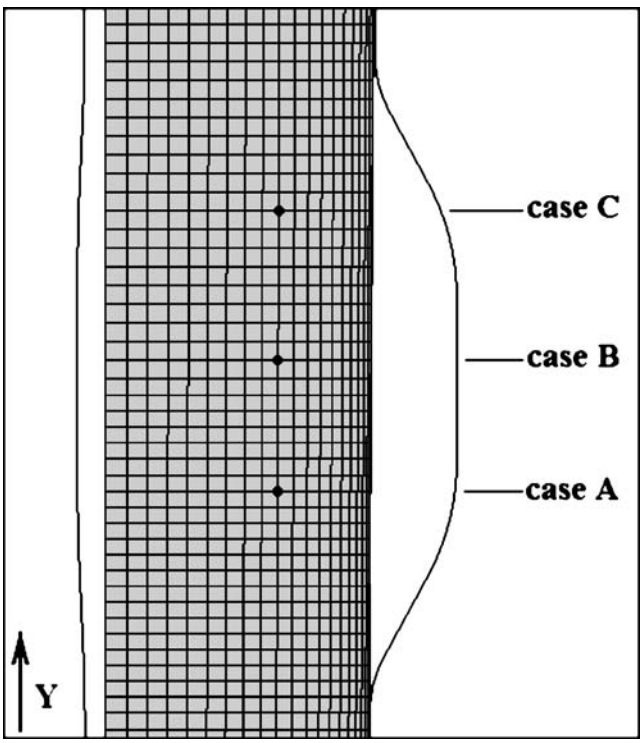

Fig. 6 Adopted positions for the weld line in the simulation

Apart from the previous dissimilar thickness models, the nominal thickness values (1.2, 1.8, and 2.4 mm) were also taken into account in the modelling of tailor-welded tubes with similar thickness. These models are useful for comparison purposes, allowing to isolate the effect of similar thickness values in the simulation, at first, but also to infer the influence of thickness on the position of the weld line in the final tubular component (weld line movement with forming). Therefore, five configurations will be numerically simulated, for each of the positions of the weld line (in Fig. 6): two with dissimilar thickness values, and the remaining three with similar nominal values for the butt tailor-welded tubes. The results obtained for the different configurations as mentioned before with the use of the EAS-based *HCi12* solid finite element described in the previous sections are presented below.

3.3.1 Case A

Case A represents a configuration with the weld line positioned at a height of 52.7 (mm) from the bottom of the initial tubular blank (Table 3). As mentioned before, three models with equal initial thickness −1.2, 1.8, and 2.4 mm (and two models with dissimilar thickness' values of 1.2×1.8 mm and 1.2×2.4) were chosen.

Figure 7 shows the thickness variation distribution after hydroforming of the tailor-welded tube relative to the original

Table 3 Weld line positions for the studied cases

Case study	Weld line location (Y position) (mm)
A	52.7
B	66.8
C	83.4

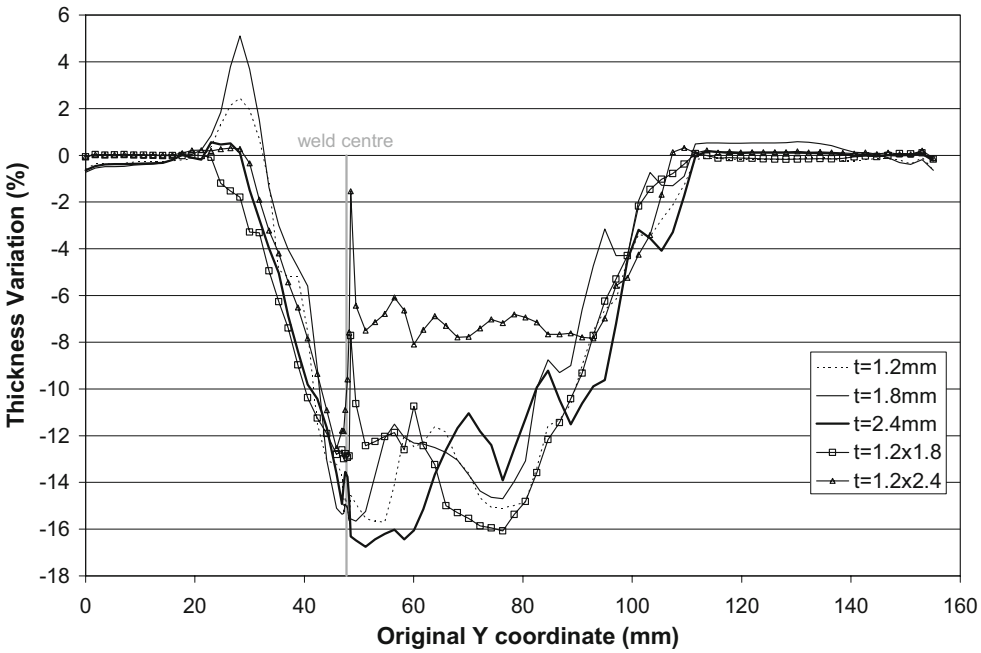

Fig. 7 Thickness distribution for case A

vertical position (Y direction in Fig. 6). Figure 7 also shows the final position of the weld-line after forming (weld center), defined as the average value from the five simulated models. The description of the weld-line movement during forming will be detailed in the following sections.

In all simulated models it can be noticed the presence of a low thickness zone in the neighbourhood of the weld line after forming. The introduction of distinct mechanical properties in the simulation is the origin of such behaviour.

From the numerical simulation analysis with the present solid-shell formulation, loading paths necessary to forming the final component can be obtained. These loading paths refer to the evolution of the input manufacture variables for a successful hydroforming, meaning, the optimal conjunction of the internal pressure field and the axial displacement imposed to the upper end of the initial tailor-welded tubular set.

The corresponding load paths for case A can be seen in Fig. 8, with imposed displacement (d) and internal pressure (P) fields for each tested models. In the figure, pressure values are expressed in MPa while displacements are shown in millimetres.

Figure 8 shows the "independent" evolutions of pressure and imposed displacement fields over the tubular blank. In the present case, the final formed configuration was achieved in five pressure/displacement steps for the similar thickness specimens. For the dissimilar thickness models, the formed part was attained after seven steps of external pressure/displacement in the numerical simulation.

Also from the graphs in Fig. 8 and for the models with dissimilar thickness, the final pressure value can be seen as a mean value of the corresponding final pressure obtained in the forming of butt tailor-welded specimens with similar thickness values. For example, the final pressure for thickness t=1.2 mm is 60 MPa, while being of 100 MPa for t=1.8 mm (and for t=2.4 mm). The observable final value for 1.2×1.8 (and also 1.2×2.4) is 80 MPa, which is derived from the numerical simulation.

Figure 9 shows the intermediate deformed configurations for the tailor-welded tube in each of the forming steps up to complete forming. Contour paths represent the evolution of the logarithmic strain in the structure. The left-hand side of each picture represents the exterior surface of the tube while the right-hand side represents the interior surface and respective strain contours.

3.3.2 Case B

The results obtained for the tailor-welded models with the weld line placed at a height of 66.8 mm are shown. This test case corresponds to case B configuration in Fig. 6. As carried out in the previous test case, three models with single thickness of 1.2, 1.8, and 2.4 mm, along with two models with dissimilar thicknesses of 1.2×1.8 mm and 1.2×2.4 mm, were considered.

Generally speaking, this model set appears with the weld line positioned at the medium height of the bulge. The distribution of thickness variation for all models belonging to case B are presented in Fig. 10, where thickness variation values are expressed related to their initial coordinates prior to the forming process.

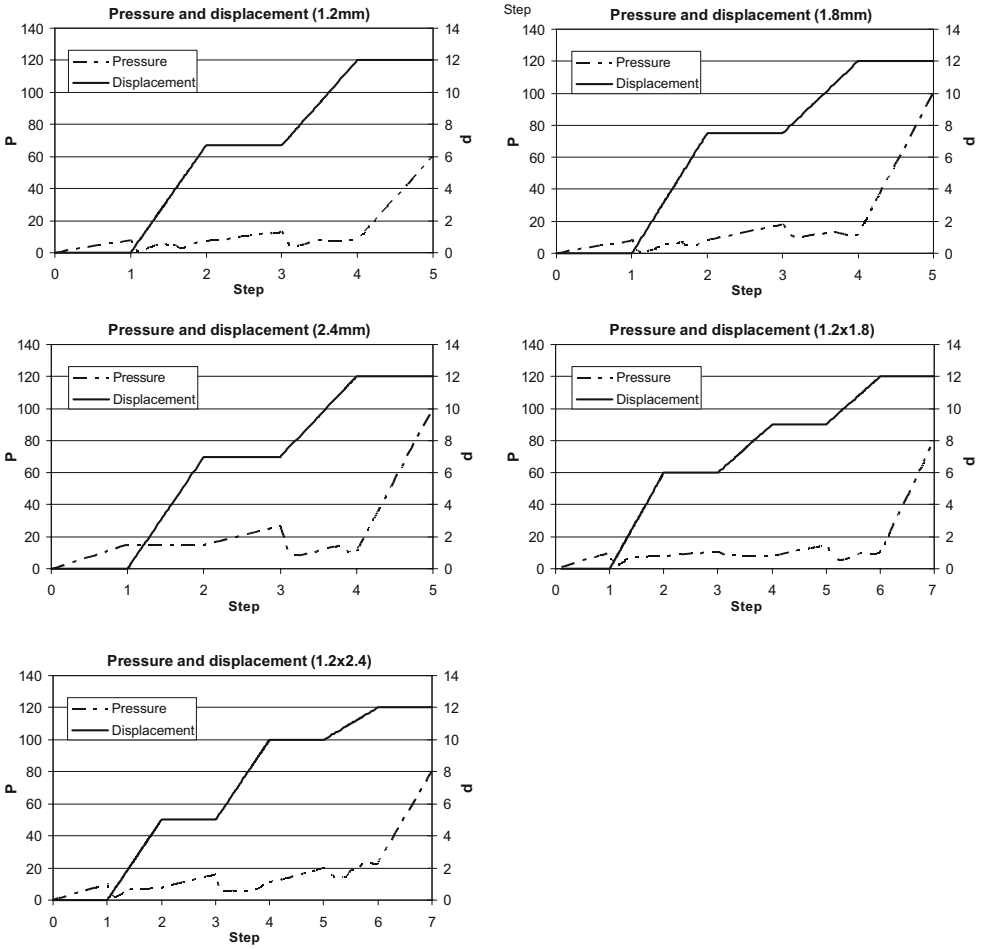

Fig. 8 Load paths (internal pressure/prescribed axial displacement) for case A (pressure in MPa, displacement in mm)

The behaviour of the models with initial constant thickness is highly similar. The largest variation in the thickness in these models occur as in the previous configuration (case A) in the neighbourhood of the weld line although the average weld line position after forming does not present relevant variations.

Figure 11 introduces the load paths obtained for the set of models in case B. In these loading paths, and following the procedure in the previous section, the evolution of the internal pressure and axial displacement imposed in the upper end of the tube are monitored. The imposed total axial displacement is kept almost unaltered in all models. The same does not happen for the final internal pressure, which changes between the considered models in order to guarantee the contact between the exterior surfaces of the tube and the die. It can be seen that for models with larger values of thickness, a further increase in the final internal pressure was needed to ensure that the complete shape is successfully obtained. All the formed shapes, excepting the one coming from the tailor-welded tube with dissimilar thickness values of 1.2×2.4 mm, were completely obtained in five steps, with distinct conjunction of internal pressure and axial feed from the simulation. The 1.2×2.4 mm tube, on the other hand, was properly formed by means of additional load increments, with the final configuration being attained after a total number of seven steps. Each forming stage, with the corresponding contours for the logarithmic strain field, is be shown in Fig. 12. As might be expected, the early formation of wrinkling zones in the earlier stages of the deformation process provides the trigger to obtain the formed final product in fewer load stages.

For the sake of completeness, a qualitative analysis of the maximum von Mises stresses can be carried out at the end of the forming process in order to infer about the influence of the dissimilar or similar thickness configurations. Maximum stress values occur in the HAZ, particularly in its geometric middle (zone 1 in Fig. 4). The higher values of stress after forming appear for dissimilar tailor-welded tubes, for configuration 1.2–2.4 (mm). Similar thickness values of the butt-welded tubes lead to lower stress values, the minimum value of stress being attained by the tube set with uniform thickness of 1.2 (mm), with an increase of the stress peak as thicknesses increase.

3.3.3 Case C

The final case study considered is case C, in which the weld line was placed at 83.4 mm for all tailor-welded models

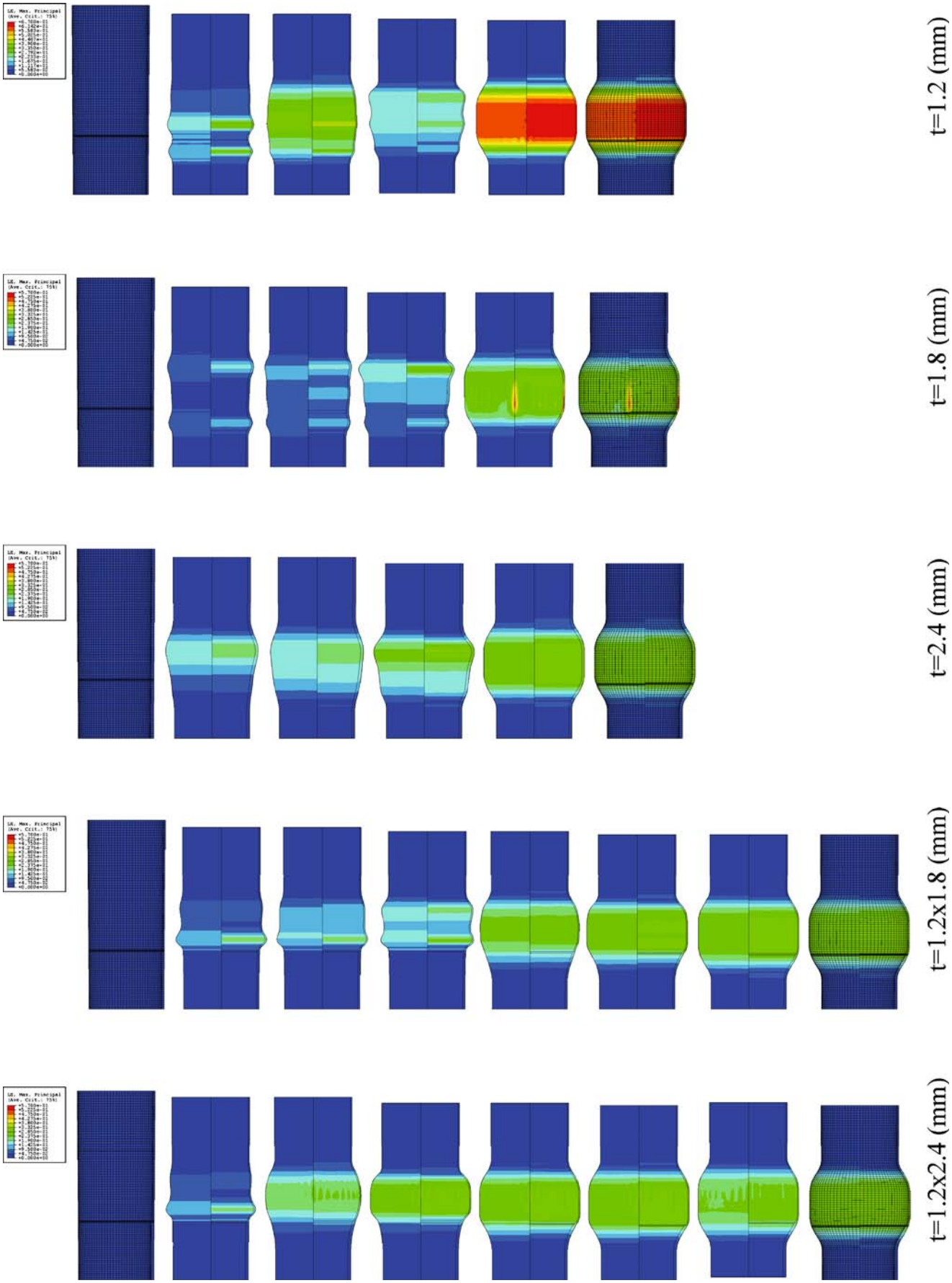

Fig. 9 Deformed configurations obtained in five (similar thickness) and seven (dissimilar thickness) steps of internal pressure and axial imposed displacement. Logarithmic strain contours are shown (case A)

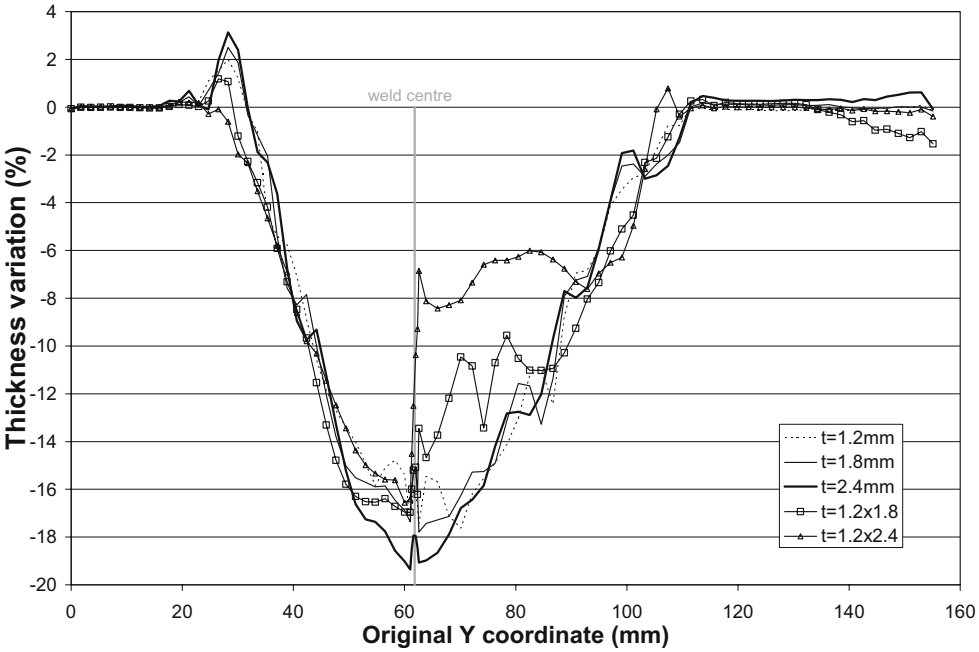

Fig. 10 Thickness distribution for case B

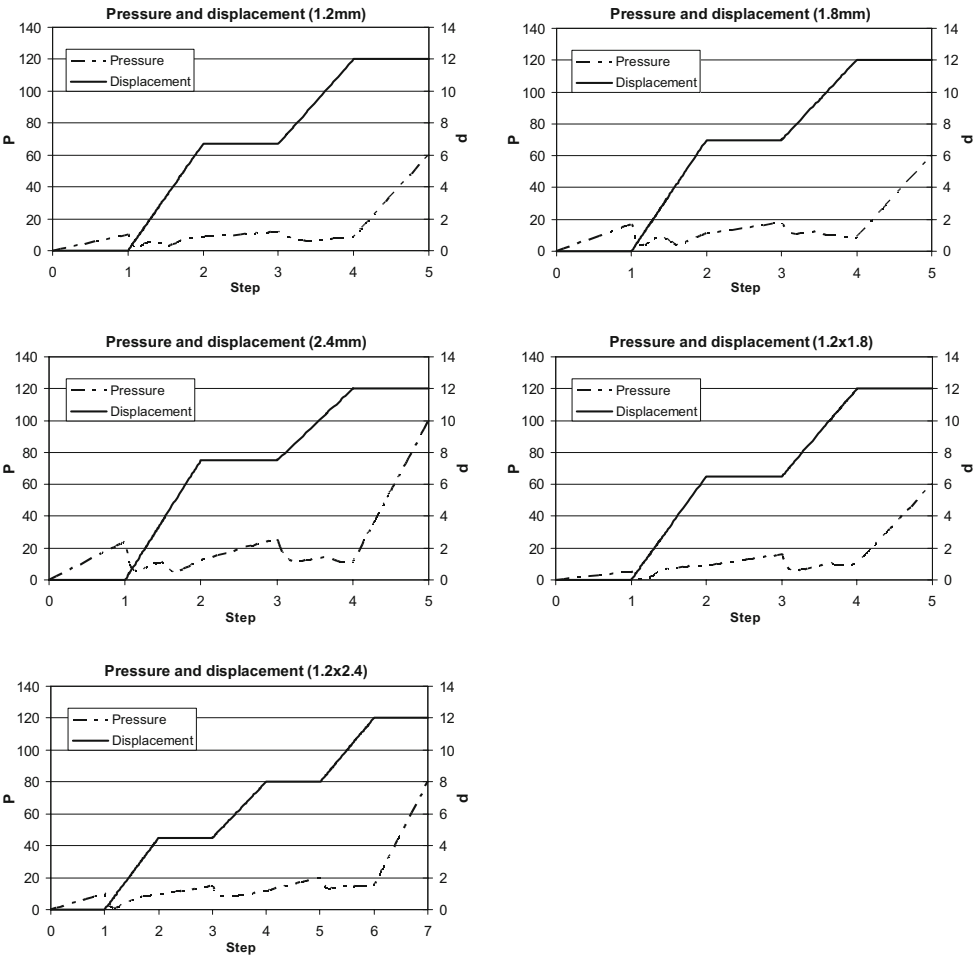

Fig. 11 Load paths (internal pressure/prescribed axial displacement) for case B (pressure in MPa, displacement in mm)

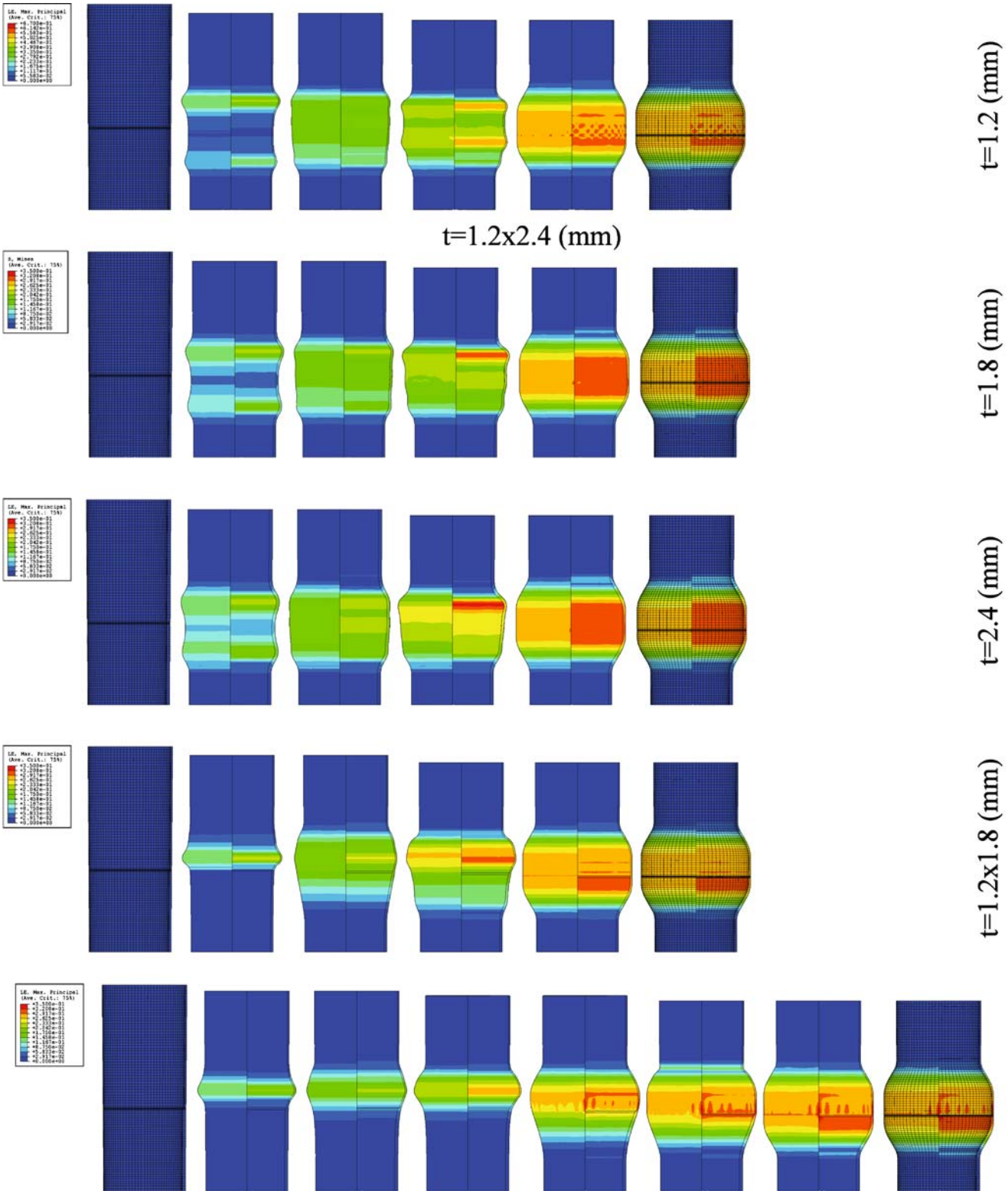

Fig. 12 Deformed configurations obtained in five and seven steps (1.2×2.4 mm) of internal pressure and axial imposed displacement. Logarithmic strain contours are shown (case B)

(Table 3). In this set of models, therefore, the weld line is positioned in the upper half of the bulge. Identical to prior cases, three single thickness and two dissimilar thickness butt-welded tubes were considered in the numerical simulation using the enhanced assumed strain solid element previously presented. The adopted thickness values are the same as in the previous sections, for cases A and B. From the results obtained by ABAQUS package, employing the

user element introduced in the present work, the evolution of thickness variation after forming, as well as the average position of the weld-line from all configurations, can be inferred from Fig. 13.

As in the previous test cases, the imposed internal pressure and axial displacements to the forming of the final part for welded configuration C, as obtained from the numerical simulation, are shown in Fig. 14. Once more it can be seen that the appearance of some models were completed in five steps while others were completed in a total of seven steps, as is the case of the tubes with dissimilar thickness. The final configurations for all models, for each forming step from simulations, and with the representation of the contours for the logarithmic strain, are shown in Fig. 15.

The model with initial single thickness of 2.4 mm shows a particular numerical behaviour during simulations, since it was not possible to fully complete the simulation due to numerical convergence problems in the final expansion step (internal pressure imposed). Nevertheless, the final part was indeed obtained after the simulation, as happened with the other models (Fig. 15), although a small gap is observed between the final component and the die walls, as can be seen in Fig. 16.

As a summary about the general aspects of the simulation, the results relative to each case (initial position of the weld line) were individually presented. The obtained results included thickness variation distribution after the forming process, as well as the strain field along the forming process, where the load paths were divided into axial displacement and internal pressure imposed on the fluid.

For these cases, the models with dissimilar thickness values presented a final pressure level similar to the model with thinnest thickness, which can be related to the fact that almost the entire tube is formed by the thinnest thickness.

The reliability of the results coming from the present numerical simulation by means of the enhanced strain solid element HCi12, as a *user-element* in ABAQUS, can be stated by comparison with results coming from that finite element commercial package itself. Among the previous variety of tailor-welded configurations, one is chosen for analysis and results for the thickness variation are seen in detail. In this sense, case B was chosen (weld-line position at 66.8 mm from the bottom of the tubular set), and dissimilar thickness values of 1.2×1.8 mm are used. The results coming from the present enhanced strain solid element are compared to those coming from ABAQUS built-in eight-node solid element C3D8. The plots of thickness variations after the complete forming are shown in Fig. 17. The picture shows very good agreement between the two sets of results, with the proposed formulation showing equivalent results than C3D8 solid element, which can infer about the predictive capabilities of the presented solid enhanced assumed strain finite element.

In the next section, a deeper study of the behaviour of the weld line is presented, focusing on its axial displacement during forming and, consequently, its position in the final formed part. This aspect is of particular interest due to considerations related to the quality of surface finishing after the hydroforming operation is completed. It will be seen that the results coming from the numerical simulation of the weld-line movement are characterized by fewer variations between the different models.

3.4 Axial displacement of the weld line

The study of weld line axial displacement, after forming, represents a very important aspect in the complete characterization of the hydroforming process of tailor-welded tubes, once it might be useful to have estimation of the amount of displacement of the weld line (and its correct position) in the final hydroformed product or at the end of intermediate forming stages.

Related to the configuration models A, B, and C discussed earlier, and from the variety of thickness values adopted, Fig. 18 summarizes the axial displacements for the weld line obtained for each distinct model, relative to each initial position.

Axial displacement of the weld-line, for each tubular configuration can be related to its initial thickness for the similar thickness configurations adopted. Table 4 shows the values of the resulting axial displacements for each different configuration as a function of the initial position of the weld line and thickness involved.

Table 5 on the other hand shows the displacements of the weld line but in this case as a function of the thickness ratio used for the butt-welded tubes with dissimilar thickness values. The ratio between the thickness values is simply considered to be the relation between the values of the thickness involved.

From the results obtained by numerical simulations of all configurations it can be seen that the variations in the weld-line movement for a fixed position of the weld-line prior to forming are relatively small between the models analysed. Nevertheless, it is relevant to mention that the initial position of the weld line has a greater influence on the weld-line displacement (for the same nominal thickness value) than the thickness value itself. It is interesting to note that this trend is verified for both the similar and dissimilar thickness butt-welded tubes.

4 Results, analysis, and discussion

In this paper, the simulation of the hydroforming process over similar and dissimilar tailor-welded tubes was carried out. Distinct configurations for the models to be formed, focusing on the initial values of thickness of the tubes and

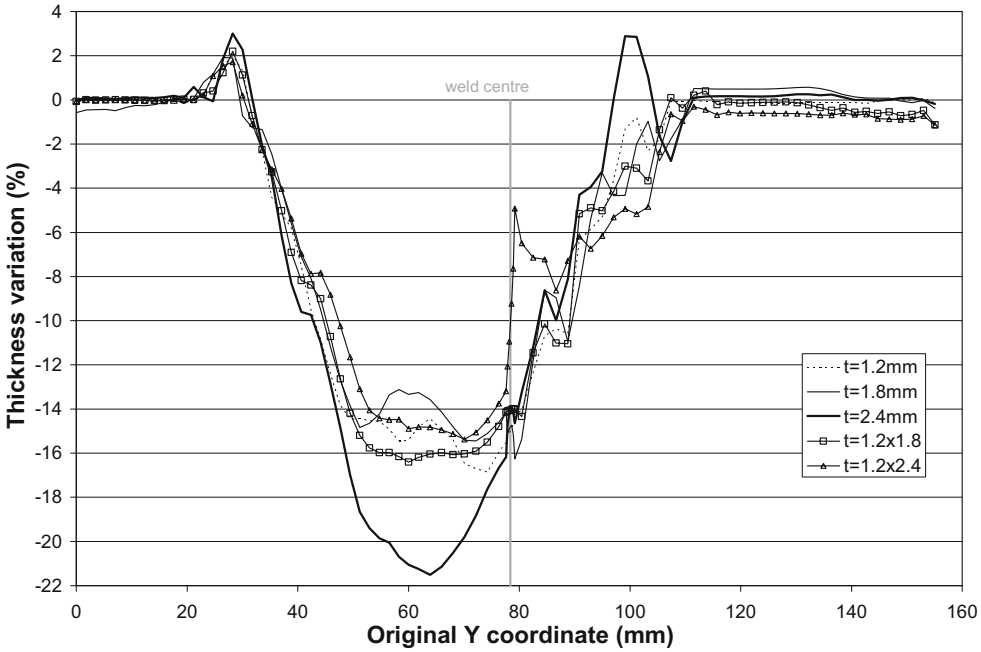

Fig. 13 Thickness distribution for case C

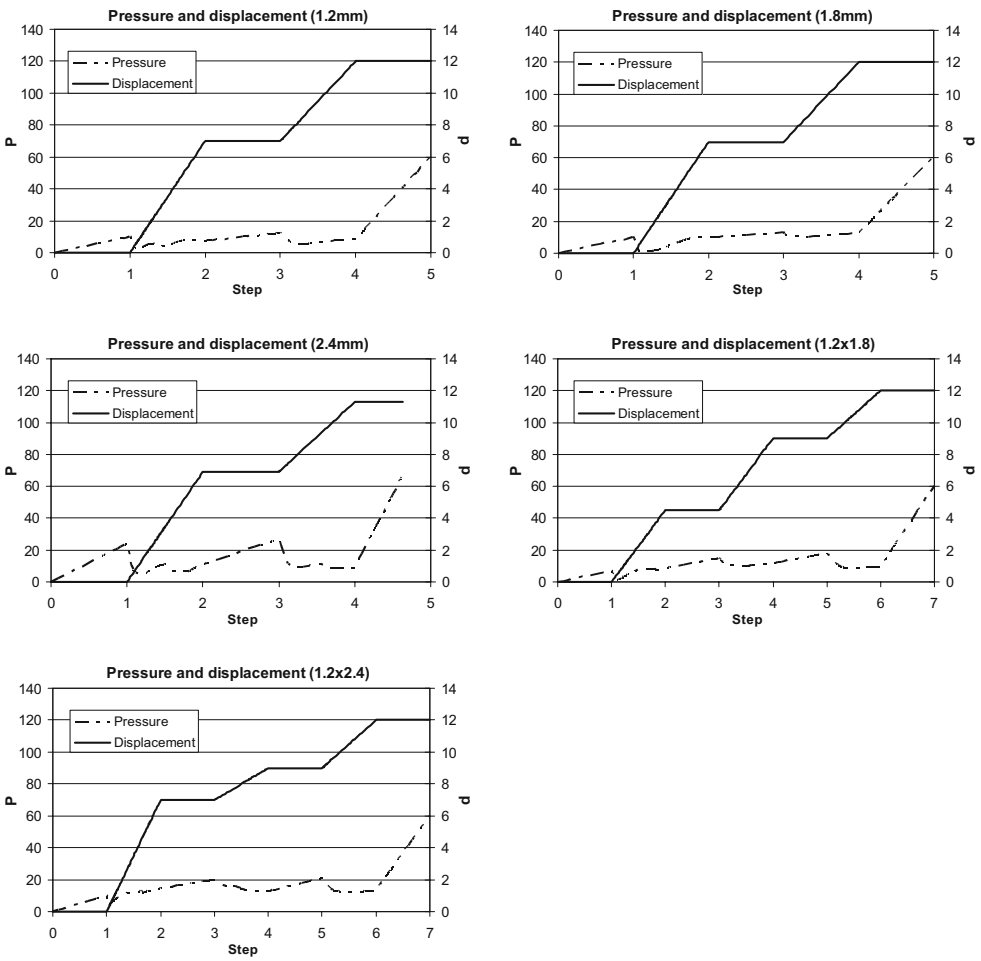

Fig. 14 Load paths (internal pressure/prescribed axial displacement) for case C (pressure in MPa, displacement in mm)

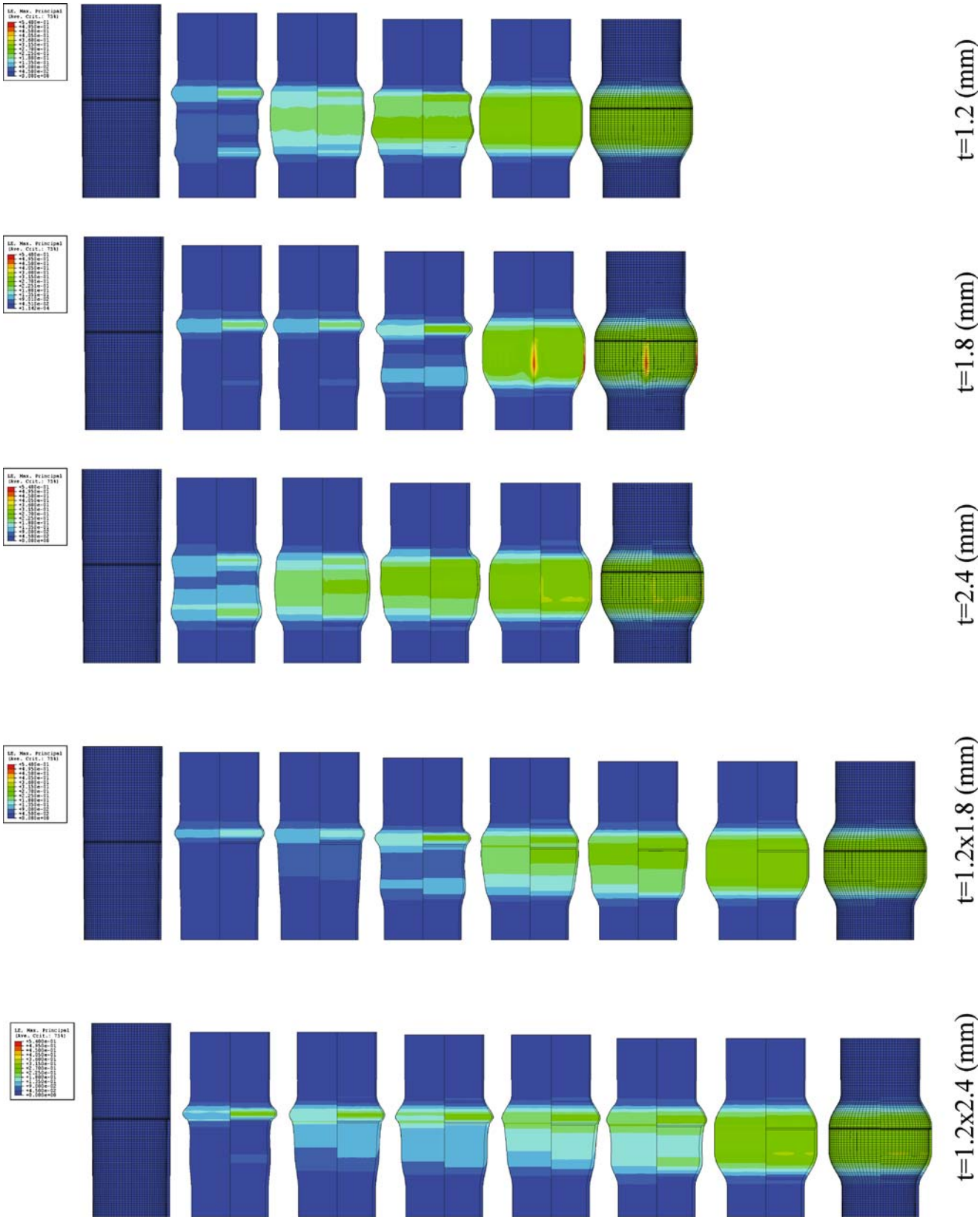

Fig. 15 Deformed configurations obtained in five (similar thickness) and seven (dissimilar thickness) steps of internal pressure and axial imposed displacement. Logarithmic strain contours are shown (case C)

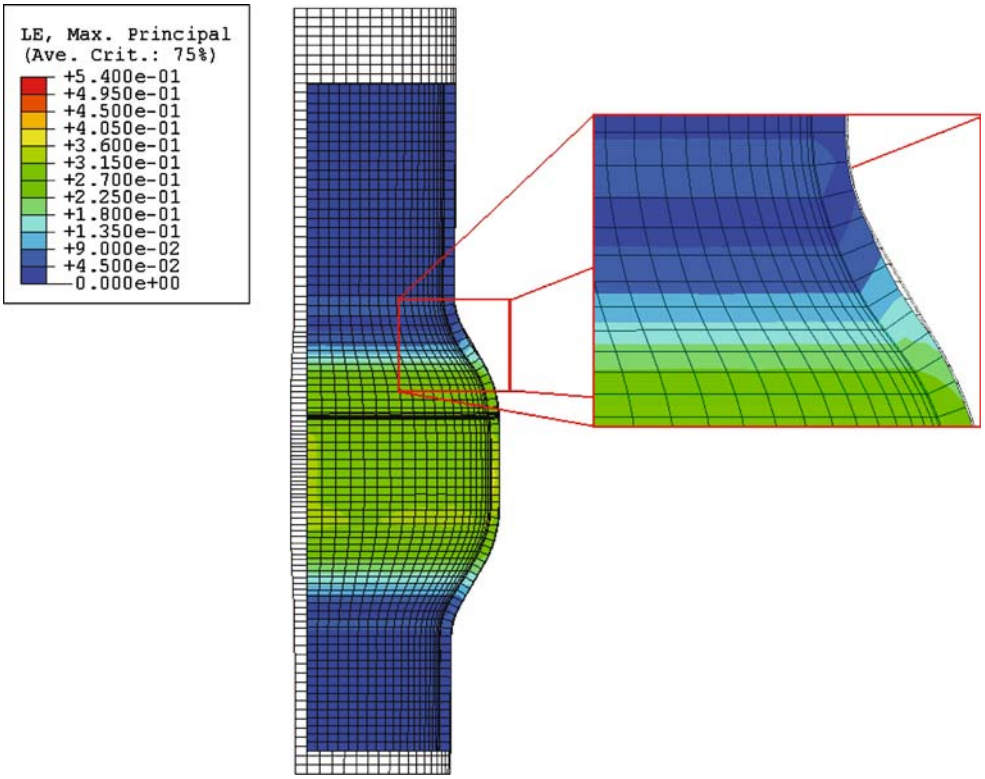

Fig. 16 Detailed view of the model with the weld line positioned at 83.4 mm (case C) and initial thickness of 2.4 (mm), for the last step from the numerical simulation

also the initial position of the weld-line, were taken into account. In this study, solid elements formulated by means of the enhanced assumed strain field were used as implemented by the authors into the finite element commercial software ABAQUS (user-elements). The main distinguishing feature of numerical models based on solid finite elements (when compared to shell or membrane finite elements) was the possibility for a more detailed and realistic description of the heat affected zone, concerning both the reproduction of mechanical properties grading and also the real geometry along the weld line. Also, thickness variation can be automatically accounted for with solid elements, which does not happen with plane stress-based finite elements. Through-thickness deformation effects,

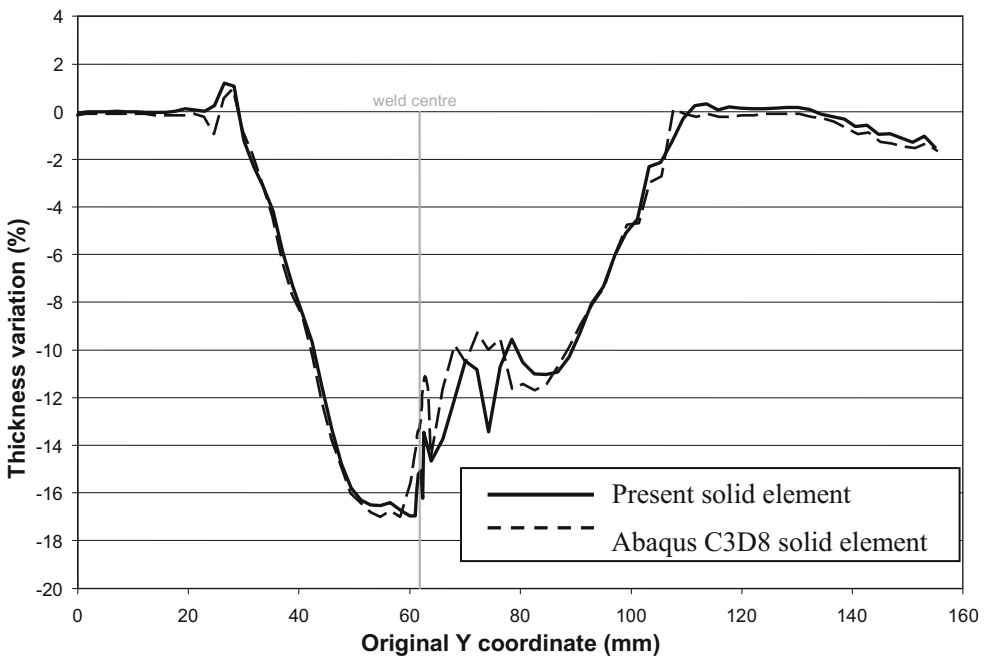

Fig. 17 Comparison of results coming from the present enhanced strain solid element (HCi12) and ABAQUS C3D8 solid element (case B, dissimilar thickness values of 1.2×1.8 mm)

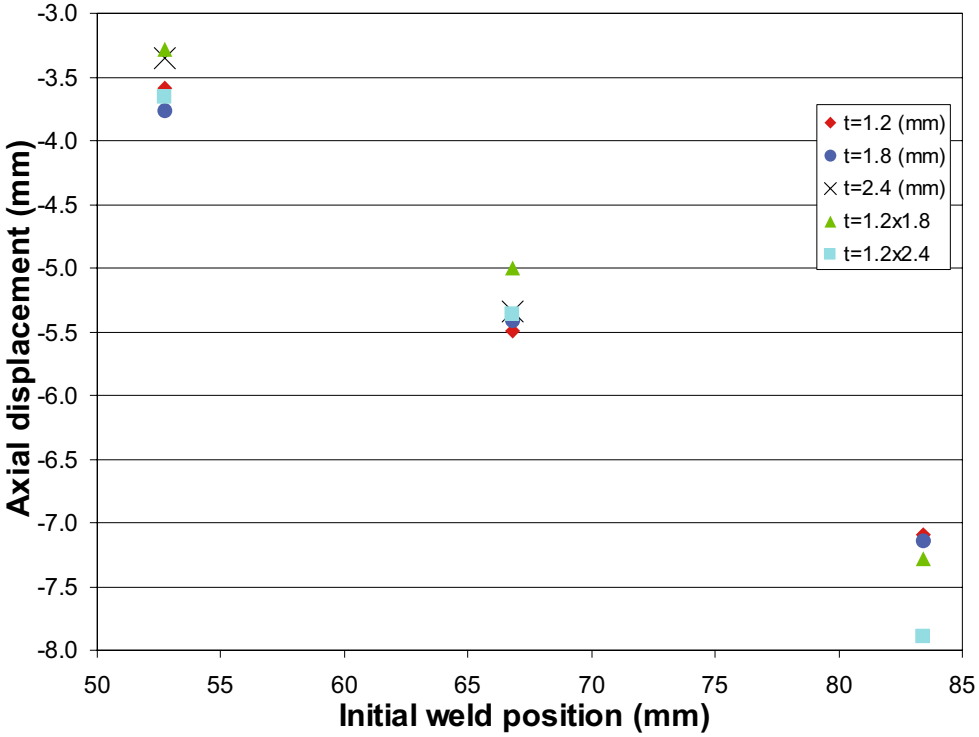

Fig. 18 Axial displacement of the weld line for different initial positions (Cases A, B, and C)

which are predominant in tubular hydroforming, can also be directly considered by the use of solid elements. This level of detail is not possible with conventional shell finite elements, and also the contact modelling between the hydroformed tube and die can be more correctly modelled with solid finite elements. The introduction of enhancing modes into the conventional finite element formulation, based on displacement-type degrees of freedom, relies on the need to avoid locking effects that appear in isochoric models of plasticity, and associated to applications with low thickness values. It was shown that the results coming from this enhanced formulation are in good agreement with results directly obtained by the ABAQUS finite element package.

For the weld-line positions considered (structural models A, B. and C), dissimilar thickness welded tubes showed the greatest thickness variation on the thick part, with this variation being greater when the thickness ratio is greater. This aspect is consistent with the higher von Mises stress level shown in dissimilar thickness models after forming. The existence of some regions where the thickness variation gradient is higher can be related to the formation of the first wrinkles, which is nevertheless necessary to subsequent forming. These are originated by instability phenomena, leading to a reduction of the thickness in the tip of the wrinkle. This local thinning effect is not completely eliminated during the process, being present in the final shape obtained. For these reasons it is clear that the process is highly dependent of the load path. In this sense, numerical simulation analysis prior to the real forming can indeed serve as a design tool for the most effective way to a complete hydroforming operation.

The axial displacement of the weld line was also studied, and the predictability character of the simulation proved to be useful. Mainly it helped to assess the relation of the weld line position (prior to forming) with its displacement during forming. It was shown that the weld line initial position has

Table 4 Axial displacement for different initial thickness configuration

h [mm]	Initial thickness [mm]		
	1.2	1.8	2.4
52.7	−3.6	−3.7	−3.3
66.8	−5.5	−5.4	−5.3
83.4	−7.1	−7.2	

Table 5 Axial displacement of the weld line for different thickness ratios

h [mm]	Ratio between thicknesses	
	1.8/1.2=1.5	2.4/1.2=2
52.7	−3.3	−3.6
66.8	−5.0	−5.4
83.4	−7.3	−7.9

a higher influence on the weld line movement after forming, than the initial thickness values involved. Nevertheless, for the models consisting of initial tubes with dissimilar thickness values, it was possible to show that the increase of the thickness ratio somewhat increases the axial displacement of the weld line resulting from the hydroforming operation.

In summary, the numerical simulation obtained with a proper finite element formulation along with a realistic description of the weld zone proved to be a useful design tool for the hydroforming process of dissimilar tailor-welded tubes. Nevertheless, some improvements in the present finite element model must be accounted for in subsequent research works, such as the inclusion of friction effects between the tube and the die walls. The influence of frictional effects into the overall movement of the welding line after forming can represent an interesting line of research, with applicability in the design of new products. Also, a more detailed constitutive law for hardening evolution in the heat affected zones, instead of the simplified model adopted in the present work, must be taken into consideration. Finally, experimental analysis for validation of the numerical models presented and proposed here will be considered in the future works of the authors.

Acknowledgments The authors would like to acknowledge the funding provided by Ministerio da Ciência, Inovação e Ensino Superior - Fundação para a Ciência e a Tecnologia (Portugal) under grants POSI SFRH/BD/13013/2003 and PTDC/EME-TME/66435/2006. Also, the funding by FEDER/FSE, with reference POCTI/EME/47289/2002 is acknowledged.

References

1. Ahmetoglu M, Sutter K, Li XJ, Altan T (2000) Tube hydroforming: current research, applications and need for training. J Mat Proc Tech 98:224–231
2. Gélin JC, Laberge C (2004) Application of optimal design and control strategies to the forming of thin walled metallic tubes. Int J Forming Proc 98:141–158
3. Jirathearanat S, Altan T (2004) Optimization of loading paths for tube hydroforming. Proc 8th Int Conf Numer Methods Industrial Forming Processes (NUMIFORM'2004). Ohio, USA
4. Dohmann F, Hartl C (1996) Hydroforming: a method to manufacture light-weighted parts. J Mat Proc Tech 60:669–676
5. Koç M, Aue-U-Lan Y, Altan T (2001) On the characterization of tubular materials for hydroforming: experimentation and analysis. Int J Machine Tool Manuf 41:761–772
6. Kim S, Kim Y (2002) Analytical study for tube hydroforming. J Mat Proc Tech 128:232–239
7. Yang B, Zhang WG, Li SH (2006) Analysis and finite element simulation of the tube bulge hydroforming process. Int J Adv Manuf Technol 29:453–458
8. Kim J, Kim SW, Park HJ, Kang BS (2006) A prediction of bursting failure in tube hydroforming process based on plastic instability. Int J Adv Manuf Technol 27:518–524
9. Roque AP, Natal Jorge RM, Parente MPL, Fontes Valente RA, Fernandes AA (2005) Hydroforming of tailor-welded tubular blanks. Proc 8th ESAFORM Conf Material Forming. Cluj-Napoca, Romania
10. Roque AP, Natal Jorge RM, Parente MPL, Fontes Valente RA, Fernandes AA (2005) Hydroforming of tailor-welded tubular blanks (2005) Proc Int Conf Numerical Methods in Engng. Granada, Spain
11. Roque AP, Natal Jorge RM, Parente MPL, Fontes Valente RA, Fernandes AA (2005) The influence of the heat affected zone on the hydroforming of tailor-welded tubular blanks (2005) Proc 8th Int Conf Comput Plasticity, Fundamentals and Applications (COMPLAS'2005). Barcelona, Spain
12. Tailor-Welded Blank Project Team (2001) Tailor-welded blank application and manufacturing: a state-of-the-art survey. The Auto/Steel Partnership http://www.a-sp.org/database/publicationmain.asp)
13. Zhao KM, Chun BK, Lee JK (2001) Finite element analysis of tailor-welded blanks. Finite El. Anal Design 37:117–130
14. Tang BT, Zhao Z, Wang Y (2007) One-step FEM-based evaluation of weld line movement and development of blank in sheet metal stamping with tailor-welded blanks. Int J Adv Manuf Technol (in press) (DOI 10.1007/s00170-006-0715-z)
15. Zhang J (2007) Optimization of contact forces in tailor-welded blanks forming process. Int J Adv Manuf Technol (in press) (DOI 10.1007/s00170-006-0491-9)
16. ABAQUS (2002) Version 6.3. Hibbitt, Karlsson & Sorensen Inc., Rhode-Island, USA
17. Harnau M, Schweizerhof K (2002) About linear and quadratic solid-shell elements at large deformations. Comp Structures 80:805–817
18. Klinkel S, Govindjee S (2002) Using finite strain 3D-material models in beam and shell elements. Eng Computat 19:902–921
19. Cardoso RPR, Yoon JW (2005) One-point quadrature shell elements for sheet metal forming analysis. Arch Comput Mech Engng 12:3–66
20. Bathe KJ (1996) Finite element procedures, 2nd edn. Prentice-Hall, New Jersey
21. Belytschko T, Liu WK, Moran B (2000) Nonlinear finite elements for continua and structures. Wiley, West Sussex, UK
22. Simo JC, Rifai MS (1990) A class of mixed assumed strain methods and the method of incompatible modes. Int J Numer Methods Eng 29:1595–1638
23. Simo JC, Armero F (1992) Geometrically non-linear enhanced strain mixed methods and the method of incompatible modes. Int. J Numer Methods Eng 3:1413–1449
24. Simo JC, Armero F, Taylor RL (1993) Improved versions of assumed enhanced strain tri-linear elements for 3D finite deformation problems. Comput Methods Appl Mech Eng 110:359–386
25. Alves de Sousa RJ, Natal Jorge RM, Fontes Valente RA, César de Sá JMA (2003) A new volumetric and shear locking-free 3D enhanced strain element. Eng Computat 20:896–925
26. Fontes Valente RA, Alves de Sousa RJ, Natal Jorge RM (2004) An enhanced strain 3D element for large deformation elastoplastic thin-shell applications. Comput Mech 34:38–52
27. Fontes Valente RA, Parente MPL, Natal Jorge RM, César de Sá JMA, Grácio JJ (2005) Enhanced transverse shear strain shell formulation applied to large elasto-plastic deformation problems. Int J Numer Methods Eng 62:1360–1398
28. Parente MPL, Fontes Valente RA, Natal Jorge RM, Cardoso RPR, Alves de Sousa RJ (2006) Sheet metal forming simulation using EAS solid-shell finite elements. Finite Elem Anal Des 42:1137–1149
29. Alves de Sousa RJ, Cardoso RPR, Valente RAF, Yoon JW, Grácio JJ, Natal Jorge RM (2005) A new one-point quadrature enhanced

assumed strain (EAS) solid-shell element with multiple integration points along thickness. Part I: Geometrically linear applications. Int J Numer Methods Eng 62:952–977

30. Alves de Sousa RJ, Cardoso RPR, Valente RAF, Yoon JW, Grácio JJ, Natal Jorge RM (2006) A new one-point quadrature enhanced assumed strain (EAS) solid-shell element with multiple integration points along thickness. Part II: Nonlinear applications. Int J Numer Methods Eng 67:160–188
31. Natal Jorge RM, Roque AP, Parente MPL, Fontes Valente RA, Fernandes AA (2004) Simulation of tubular hydroforming. Proc 4th Int Conf Engineering and Computational Technology. Lisbon, Portugal
32. Reis AR, Teixeira P, Ferreira Duarte J, Santos A, Barata da Rocha A, Fernandes AA (2004) Tailored welded blanks–an experimental and numerical study in sheet metal forming on the effect of welding. Comp Struct 82:1435–1442